scientific reports

OPEN

Variational quantum metrology for multiparameter estimation under dephasing noise

Trung Kien Le[1,2], Hung Q. Nguyen[3] & Le Bin Ho[4,5✉]

We present a hybrid quantum-classical variational scheme to enhance precision in quantum metrology. In the scheme, both the initial state and the measurement basis in the quantum part are parameterized and optimized via the classical part. It enables the maximization of information gained about the measured quantity. We discuss specific applications to 3D magnetic field sensing under several dephasing noise models. Indeed, we demonstrate its ability to simultaneously estimate all parameters and surpass the standard quantum limit, making it a powerful tool for metrological applications.

Quantum metrology is an estimation process that utilizes unique quantum phenomena such as entanglement and squeezing to improve the precision of estimation beyond classical limits[1–3]. Recent development in quantum computing leads to numerous optimal algorithms for enhancing precision in single-parameter estimation, such as adaptive measurements[4–7], quantum error correction[8,9], and optimal quantum control[10–12]. So far, a variational algorithm has been demonstrated by combining the advantages of both quantum and classical systems for quantum-enhanced metrology[12–15]. A similar protocol for spin systems was also introduced[16,17].

Multiparameter estimation is essential in various fields, such as Hamiltonian tomography[18], multiphase sensing[19–21], gravitational wave detection[22], and atomic clocks[23,24]. However, the estimation is more challenging due to the incompatibility[25]. In these cases, simultaneous determination of all parameters is impossible, resulting in a tradeoff[26]. Numerous techniques have been introduced to tackle this challenge, including establishing optimal measurement strategies[27,28], employing parallel scheme[21], sequential feedback scheme[29], and implementing post-selection procedures[30]. More recently, a variational toolbox for multiparameter estimation was proposed[31], which is a generalization from the previous work mentioned above[14].

While using variational schemes is promising, their potential significance in multiparameter quantum metrology has yet be fully understood, even in principle. Furthermore, determining the optimal quantum resources and measurement strategy to extract maximum information about all parameters is limited by the tradeoffs in estimating incompatible observables[26,32,33] and required collective measurements over multiple copies of a probe state[32,33]. Therefore, finding a suitable and practical strategy for precise estimation of multiple parameters remains a thriving area of quantum metrology.

In this work, we propose a variational scheme to enhance the precision of multiparameter estimation in the presence of dephasing noise. The basic idea is to use a quantum computer to prepare a trial state (an ansatz) that depends on a set of trainable variables. The state is subjected to a series of control operations, representing unknown multiparameter and noise, and then is measured through observables determined by other trainable variables. The measurement results are used to update the trainable variables and optimize the estimation of the unknown parameters.

Optimizing both the initial probe state and the measurement operators allows us to identify suitable conditions for the quantum probe to increase sensitivity and achieve the ultimate quantum limit for all parameters. In numerical simulations, we estimate a 3D magnetic field under a dephasing noise model and find that sensitivity for all parameters can simultaneously reach the ultimate quantum bound, i.e., the classical bound equals the quantum bound. We also examine a time-dependent Ornstein-Uhlenbeck model[34] and observe results surpassing the standard quantum limit by increasing the probe's number of particles. This approach holds promise for a wide range of metrological applications, including external field sensing, precision spectroscopy, gravitational wave detection, and others, where the effects of noises cannot be ignored.

[1]Department of Physics, University of California, Santa Barbara, Santa Barbara, USA. [2]Present address: Department of Applied Physics, Stanford University, Stanford, California 94305, USA. [3]Nano and Energy Center, University of Science, Vietnam National University, Hanoi 120401, Vietnam. [4]Frontier Research Institute for Interdisciplinary Sciences, Tohoku University, Sendai 980-8578, Japan. [5]Department of Applied Physics, Graduate School of Engineering, Tohoku University, Sendai 980-8579, Japan. ✉email: binho@fris.tohoku.ac.jp

Results

Variational quantum metrology

The goal of multiparameter estimation is to evaluate a set of unknown d parameters $\boldsymbol{\phi} = (\phi_1, \phi_2, \ldots, \phi_d)^\mathsf{T}$, which are imprinted onto a quantum probe via a unitary evolution $\boldsymbol{U}(\boldsymbol{\phi}) = \exp(-it\boldsymbol{H}\boldsymbol{\phi}) = \exp(-it\sum_{k=1}^d H_k\phi_k)$, where $\boldsymbol{H} = (H_1, H_2, \ldots, H_d)$ are non-commuting Hermitian Hamiltonians. The precision of estimated parameters $\boldsymbol{\phi}$ is evaluated using a mean square error matrix (MSEM) $V = \sum_m p(m|\boldsymbol{\phi})[\check{\boldsymbol{\phi}}(m) - \boldsymbol{\phi}][\check{\boldsymbol{\phi}}(m) - \boldsymbol{\phi}]^\mathsf{T}$, where $p(m|\boldsymbol{\phi}) = \mathrm{Tr}[\rho(\boldsymbol{\phi})E_m]$ is the probability for obtaining an outcome m when measuring the final state $\rho(\boldsymbol{\phi})$ by an element E_m in a positive, operator-value measure (POVM). For unbiased estimators, the MSEM obeys the Cramér-Rao bounds (CRBs)[35–38]

$$\mathrm{Tr}[WV] \geq \mathsf{C_F} \geq \mathsf{C_{NH}} \geq \mathsf{C_H} \geq \mathsf{C_S}, \tag{1}$$

where W is a scalar weight matrix, which can be chosen as an identity matrix without loss of generality. The classical bound is $\mathsf{C_F} = \mathrm{Tr}[WF^{-1}]$, where F is the classical Fisher information matrix (CFIM) with elements $F_{ij} = \sum_m \frac{1}{p(m|\boldsymbol{\phi})}[\partial_{\phi_i} p(m|\boldsymbol{\phi})][\partial_{\phi_j} p(m|\boldsymbol{\phi})]$[39]. The Nagaoka–Hayashi bound $\mathsf{C_{NH}}$ and Holevo bound $\mathsf{C_H}$ are given via semidefinite programming, i.e., $\mathsf{C_{NH}} = \min_{\{D,X\}} \mathrm{Tr}[(W \otimes \rho(\boldsymbol{\phi})) \cdot D]$[38,40], and $\mathsf{C_H} = \min_{\{X\}}(\mathrm{Tr}[W\mathrm{Re}Z + ||\sqrt{W}\mathrm{Im}Z\sqrt{W}||_1)$[36,41], where D is a d-by-d matrix contains Hermitian operators D_{ij} and satisfies $D \geq XX^\mathsf{T}$, $X = (X_1, X_2, \ldots, X_d)^\mathsf{T}$ satisfies $\mathrm{Tr}[\rho(\boldsymbol{\phi})X_j] = \phi_j$ and $\mathrm{Tr}[X_i\partial_{\phi_j}\rho(\boldsymbol{\phi})] = \delta_{ij}$, Z is a positive semidefinite matrix with elements $Z_{ij} = \mathrm{Tr}[X_iX_j\rho(\boldsymbol{\phi})]$. Finally, $\mathsf{C_S} = \mathrm{Tr}[WQ^{-1}]$ is a symmetric logarithmic derivative (SLD) quantum bound where $Q_{ij} = \mathrm{Re}[\mathrm{Tr}[\rho(\boldsymbol{\phi})L_iL_j]]$ is the real symmetric quantum Fisher information matrix (QFIM) that defined through the SLD $2\partial_{\phi_j}\rho(\boldsymbol{\phi}) = \{L_j, \rho(\boldsymbol{\phi})\}$[39].

Although optimal estimators can achieve $\mathsf{C_F}$[42], the $\mathsf{C_{NH}}$ can be attainted with separable measurements for qubits probes[40], and asymptotic achievement of $\mathsf{C_H}$ is possible[43–47], it is not always possible to attain $\mathsf{C_S}$ for multiparameter estimation[41]. In this work, we attempt to reach this bound. In some instances, $\mathsf{C_H} = \mathsf{C_S}$ if a weak commutativity condition $\mathrm{Im}(\mathrm{Tr}[L_jL_i\rho(\boldsymbol{\phi})]) = 0$ is met[41,48]. A similar condition for pure states is also applied to attain $\mathsf{C_F} = \mathsf{C_S}$[19,49,50]. Further discussion on the interplay between $\mathsf{C_{NH}}$, $\mathsf{C_H}$, and $\mathsf{C_S}$ has been reported[37]. However, this condition alone is insufficient to achieve the quantum bounds practically; instead, attaining $\mathsf{C_S}$ and $\mathsf{C_H}$ also requires entangled measurements (POVM) over multiple copies[45,46]. Recently, Yang et al., have derived saturation conditions for general POVMs[28]. To be more precise, when $F \geq Q > 0$ and for any arbitrary full-rank positive weight matrix $W > 0$, the equally $\mathsf{C_F} = \mathsf{C_S}$ implies $F = Q$.

This paper presents a variational quantum metrology (VQM) scheme following Meyer et al. toolbox[31] as sketched in Fig. 1 to optimize both the preparation state and POVM. A quantum circuit $\boldsymbol{U}(\boldsymbol{\theta})$ is used to generate a variational preparation state with trainable variables $\boldsymbol{\theta}$. Similar quantum circuit with variables $\boldsymbol{\mu}$ is used to generate a variational POVM $\boldsymbol{E}(\boldsymbol{\mu}) = \{E_m(\boldsymbol{\mu}) = \boldsymbol{U}^\dagger(\boldsymbol{\mu})E_m\boldsymbol{U}(\boldsymbol{\mu}) > 0 | \sum_m E_m(\boldsymbol{\mu}) = I\}$. Using classical computers, a cost function $\mathcal{C}(\boldsymbol{\theta}, \boldsymbol{\mu})$ can be optimized to update the variables for quantum circuits, resulting in enhanced information extraction. The scheme is repeated until it converges.

To investigate the attainable the ultimate SLD quantum bound, we define the cost function by a relative difference[47]

$$\mathcal{C}(\boldsymbol{\theta}, \boldsymbol{\mu}) = 1 - \frac{\mathsf{C_S}}{\mathsf{C_F}}, \tag{2}$$

which is positive semidefinite according to Eq. (1). The variables are trained by solving the optimization task $\arg\min_{\{\boldsymbol{\theta}, \boldsymbol{\mu}\}} \mathcal{C}(\boldsymbol{\theta}, \boldsymbol{\mu})$. As the value of $\mathcal{C}(\boldsymbol{\theta}, \boldsymbol{\mu})$ approaches zero, we reach the ultimate SLD quantum bound where $\mathsf{C_F} = \mathsf{C_S}$. Notably, we strive for agreement between classical and SLD quantum bounds assuming $\mathrm{Tr}[WV] = \mathsf{C_F}$, and thus, omit discussion on the estimator for achieving $\mathrm{Tr}[WV] = \mathsf{C_F}$. Moreover, the cost function (2) serves as a technical tool to optimize the variational scheme, while the main analyzing quantities are CRBs. A vital feature of the VQM is using variational quantum circuits, which allows for optimizing the entangled probe state and measurements to extract the maximum information about the estimated parameters. This approach thus
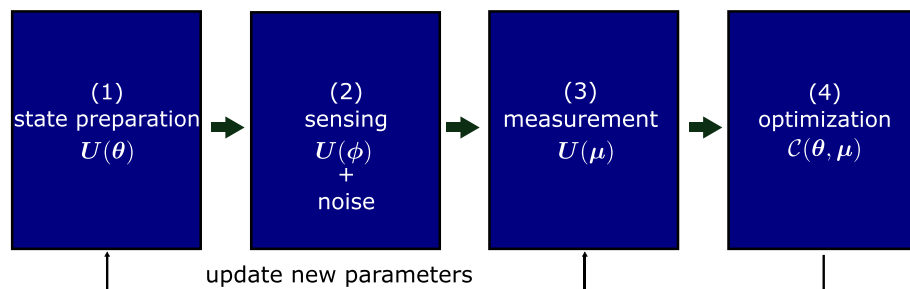

Figure 1. Variational quantum metrology. (1) use quantum circuit $\boldsymbol{U}(\boldsymbol{\theta})$ to prepare a variational state; (2) encode multiparameter $\boldsymbol{\phi}$ and noise using $\boldsymbol{U}(\boldsymbol{\phi})$ and noise channels; (3) use circuit $\boldsymbol{U}(\boldsymbol{\mu})$ to create a variational POVM for measurement; (4) send measurement results to a classical computer to optimize cost function $\mathcal{C}(\boldsymbol{\theta}, \boldsymbol{\mu})$ using a gradient-based optimizer. Update new training variables and repeat the scheme until it converges.

does not require entangled measurements over multiple copies. We further discuss various cost functions in the Discussion section.

Ansatzes

We propose three variational circuits: a star topology ansatz, a ring topology ansatz, and a squeezing ansatz. The first two ansatzes are inspired by quantum graph states, which are useful resources for quantum metrology[51,52]. A conventional graph state is formed by a collection of vertices V and edges D as $G(V, D) = \prod_{i,j \in D} CZ^{ij} |+\rangle^V$, where CZ^{ij} represents the controlled-Z gate connecting the i and j qubits, and $|+\rangle$ is an element in the basis of Pauli σ_x. The proposed ansatzes here incorporate y-rotation gates ($R_y(\theta) = e^{-i\theta\sigma_y/2}$) at every vertex prior to CZ gates (see Fig. 2a,b). The squeezing ansatz in Fig. 2c is inspired by squeezing states, which is another useful resource for quantum metrology[53–55]. It has $x(y)$-rotation gates and global Mølmer–Sørensen gates $U_{x(z)}$, where $U_{x(z)} = \exp(-i \sum_{j=1}^{N} \sum_{k=j+1}^{N} \sigma_{x(z)} \otimes \sigma_{x(z)} \frac{\chi_{jk}}{2})$ for an N-qubit circuit[56]. The trainable variables for one layer are $2N - 2$, $2N$, and $N(N + 1)$ for the star, ring, and squeezing ansatz, respectively. Hereafter, we use these ansatzes for generating variational preparation states and variational POVM in the VQM scheme.

Multiparameter estimation under dephasing noise

After preparing a variational state $\rho(\boldsymbol{\theta}) = U(\boldsymbol{\theta})\rho_0 U(\boldsymbol{\theta})$, we use it to estimate a 3D magnetic field under dephasing noise. The field is imprinted onto every single qubit via the Hamiltonian $\boldsymbol{H} = \sum_{i \in \{x,y,z\}} \phi_i \sigma_i$, where $\boldsymbol{\phi} = (\phi_x, \phi_y, \phi_z)$, and σ_i is a Pauli matrix. Under dephasing noise, the variational state $\rho(\boldsymbol{\theta})$ evolves to[13]

$$\mathcal{E}_t(\rho) = \left[\prod_{k=1}^{N} e^{\gamma t \mathcal{L}^{(k)}} \right] e^{-it\mathcal{H}} \rho, \tag{3}$$

where we omitted $\boldsymbol{\theta}$ in $\rho(\boldsymbol{\theta})$ for short. The superoperator $\mathcal{H}$ generates a unitary dynamic $\mathcal{H}\rho = [\boldsymbol{H}, \rho]$, and $\mathcal{L}^{(k)}$ is a non-unitary dephasing superoperator with γ is the decay rate. In terms of Kraus operators, the dephasing superoperator gives

$$e^{\gamma t \mathcal{L}^{(k)}} \rho = K_1^{(k)} \rho [K_1^{(k)}]^\dagger + K_2^{(k)} \rho [K_2^{(k)}]^\dagger, \tag{4}$$

where $K_1 = \begin{pmatrix} \sqrt{1-\lambda} & 0 \\ 0 & 1 \end{pmatrix}$ and $K_2 = \begin{pmatrix} \sqrt{\lambda} & 0 \\ 0 & 0 \end{pmatrix}$ are Kraus operators, and $\lambda = 1 - e^{-\gamma t}$ is the dephasing probability. Finally, the state is measured in the variational POVM $E(\boldsymbol{\mu})$ and yields the probability $p(m) = \text{Tr}[\mathcal{E}_t(\rho) E_m(\boldsymbol{\mu})]$. Note that p also depends on $\boldsymbol{\theta}, \boldsymbol{\phi}$, and $\boldsymbol{\mu}$.

It is important to attain the ultimate SLD quantum bound, i.e., $\mathsf{C_F} = \mathsf{C_S}$. We thus compare numerical results for the cost function, $\mathsf{C_F}$, and $\mathsf{C_S}$ as shown in the top panels of Fig. 3. At each λ, the cost function and other quantities are plotted with the optimal θ obtained after stopping the training by EarlyStopping callback[57]. The numerical results are presented at $N = 3$, and the number of layers is chosen from their optimal values as shown in the Method and Fig. 8. Through the paper, we fixed $(\phi_x, \phi_y, \phi_z) = (\pi/6, \pi/6, \pi/6)$.

We find that for small noises, $\mathsf{C_F}$ reaches $\mathsf{C_S}$, which is consistent with earlier numerical findings[46,47]. Remarkably, different from the previous findings where the convergence of these bounds is not clear, here we show that both $\mathsf{C_F}$ and $\mathsf{C_S}$ remain small (also in comparison to previous work[31]) without any divergence. We further compare the performance of the star ansatz to that of the ring and squeezing ansatzes. It saturates the ultimate quantum limit for dephasing probabilities $\lambda < 0.5$, whereas the ring and squeezing ansatzes only reach the limit for $\lambda < 0.2$. The reason is that the star graph exhibits a central vertex connected to the remaining $N - 1$ surrounding vertices, which facilitates robust quantum metrology, as discussed in[51].

Furthermore, we evaluate the tradeoff between the CFIM and QFIM by introducing a function $\mathcal{T} = \text{Tr}[FQ^{-1}]$. For unknown d parameters, the naive bound is $\max(\mathcal{T}) = d$, leading to simultaneous optimization of all parameters. The results are shown in the bottom panels of Fig. 3 and agree well with the CRBs presented in the top panels, wherein $\mathcal{T} \to 3$ whenever the SLD quantum bound is reached. So far, we observe that $\mathcal{T} > d/2$ for all cases, which is better than the theoretical prediction previously[58]. This observation exhibits a practical advantage of the VQM approach across different levels of noise.
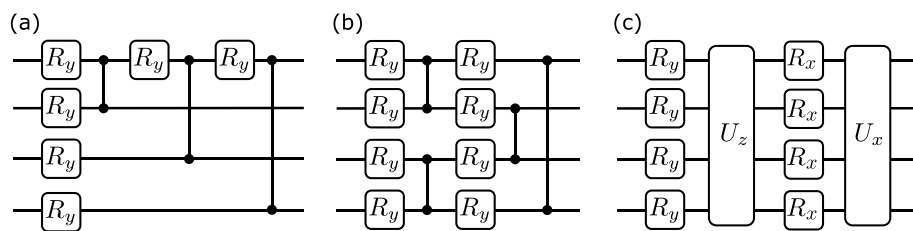

Figure 2. Ansatzes for preparation state and POVM. (**a**) Star topology entangled ansatz. (**b**) Ring topology entangled ansatz. (**c**) Squeezing ansatz. In the circuits, $R_{x(y)}$: $x(y)$-rotation gate, $U_{x(z)}$: global Mølmer–Sørensen gate, ●–●: controlled-Z gate.

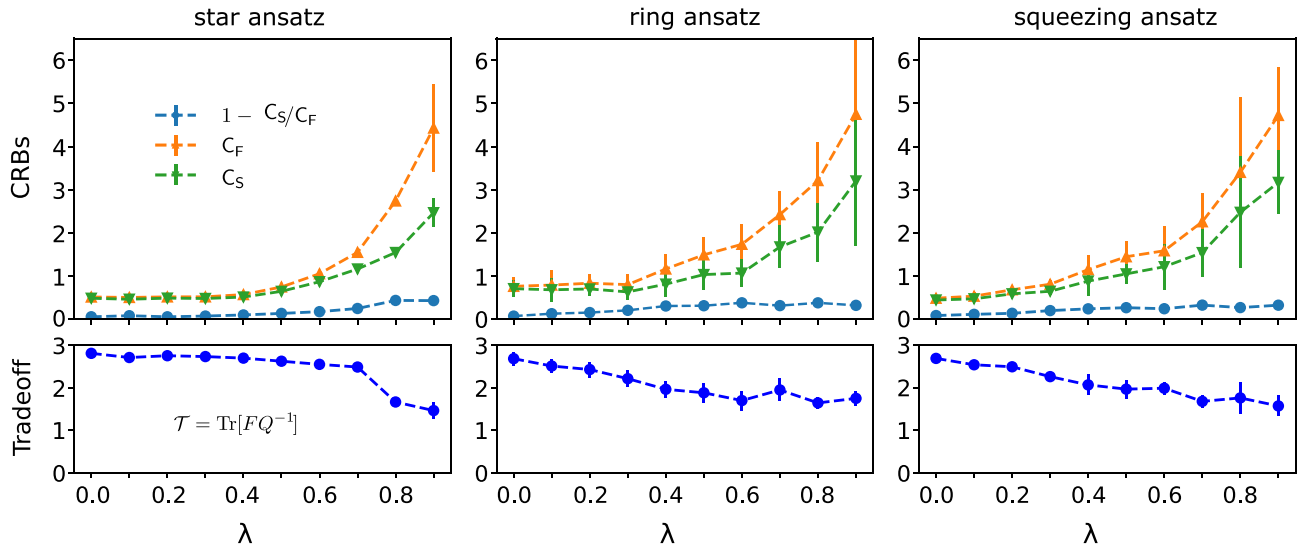**Figure 3.** Variational quantum metrology under dephasing noise. (Top): plot of the optimal cost function $\mathcal{C}(\boldsymbol{\theta}, \boldsymbol{\mu})$, classical bound C_F, and SLD quantum bound C_S as functions of dephasing probability. From left to right: star, ring, and squeezing ansatz. (Bottom): plot of corresponding tradeoff $\mathcal{T}$. Numerical results are calculated at $N = 3$, the optimal number of layers in Fig. 8, and the results are averaged after 10 samples.

Barren plateaus

Variational quantum circuits under the influence of noises will exhibit a barren plateau (BP), where the gradient along any direction of the variables' space vanishes exponentially with respect to the noise level[59]. The BP prevents reaching the global optimization of the training space, thereby reducing the efficiency and trainability of the variational quantum circuit. However, BPs can be partially mitigated through carefully designing ansatzes and cost functions[60].

The deviation of CRBs shown in Fig. 3 may be subject to the BP raised by noise. We examine such dependent and show the results in Fig. 4. We plot $|\partial_{\theta_1} \mathcal{C}|$ (Fig. 4a) and $\mathrm{Var}[\partial_{\theta_1} \mathcal{C}]$ (Fig. 4b), where $\mathcal{C}$ is defined in Eq. (2) after 200 runs with random initialization of $\boldsymbol{\theta}$ and $\boldsymbol{\mu}$ for each value of λ. As predicted, both of them demonstrate an exponential decline with an increase in the dephasing probability. Especially, $\mathrm{Var}[\partial_{\theta_1} \mathcal{C}]$ exponentially vanishes with the slope of -2.259, -2.533, and -3.240 for the star, ring, and squeezing ansatz, respectively. The star ansatz exhibits slower gradient decay as λ approaches 1 due to its smaller trainable variables' space than the ring and squeezing ansatz. This indicates better training and less susceptibility to vanishing gradients, leading to better achievement of the ultimate quantum bound.
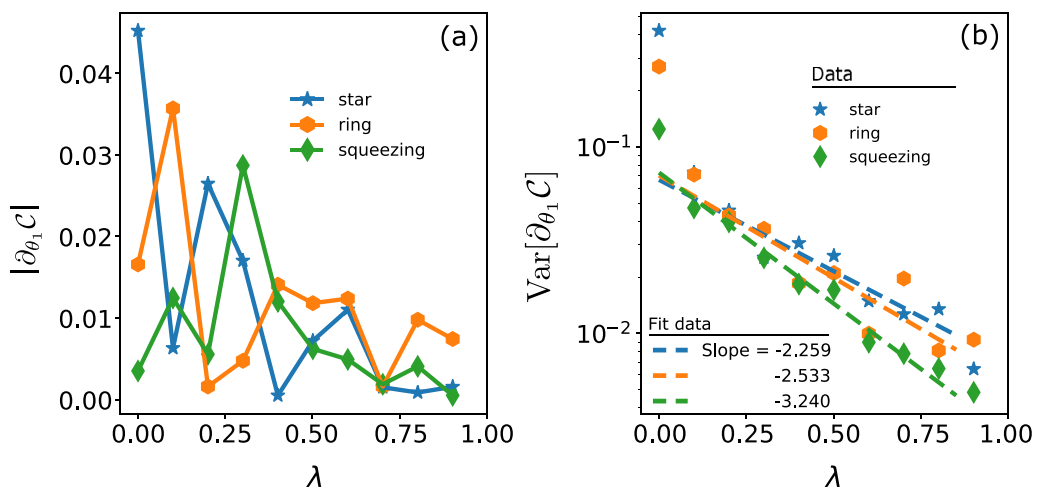

Figure 4. Barren plateau. (**a**) Plot of $|\partial_{\theta_1} \mathcal{C}|$ as a function of the dephasing probability λ. (**b**) Plot of the variance of gradient $\mathrm{Var}[\partial_{\theta_1} \mathcal{C}]$. The slope of each fit line indicates the exponential decay of the gradient, which is a sign of the barren plateau effect. The results are taken average after 200 runs.

Multiparameter estimation under the Ornstein–Uhlenbeck model

We consider the Ornstein-Uhlenbeck model, where the noise is induced by the stochastic fluctuation of the external (magnetic) field[34]. The Kraus operators are[61]

$$K_1(t) = \begin{pmatrix} \sqrt{1-q(t)} & 0 \\ 0 & 1 \end{pmatrix}, \; K_2(t) = \begin{pmatrix} \sqrt{q(t)} & 0 \\ 0 & 0 \end{pmatrix},$$

(5)

where $q(t) = 1 - e^{-f(t)}$ with $f(t) = \gamma[t + \tau_c(e^{-t/\tau_c} - 1)]$, and τ_c represents the memory time of the environment. In the Markovian limit ($\tau_c \to 0$), $f(t) = \gamma t$, which corresponds to the previous dephasing case. In the non-Markovian limit with large τ_c, such as $t/\tau_c \ll 1$, we have $f(t) = \frac{\gamma t^2}{2\tau_c}$. In the numerical simulation, we fixed $\gamma = 0.1$ and $\tau_c = 20$ (for non-Markovian)

$$q(t) = \begin{cases} 1 - \exp(-0.1t) & \text{Markovian,} \\ 1 - \exp(-\frac{t^2}{400}) & \text{non-Markovian.} \end{cases}$$

(6)

We use this model to study the relationship between sensing time, Markovianity, and ultimate attainability of the quantum bound. Figure 5a displays the optimal CRBs for Markovian and non-Markovian noises as functions of sensing time t. As previously reported in[20], there exists an optimal sensing time that minimizes the CRBs for each case examined here. Moreover, the non-Markovian dephasing (nMar) results in lower metrological bounds as compared to the Markovian case (Mar). So far, the minimum CRBs for different N are presented in Fig. 5b. The results demonstrate that with an increase in N, the non-Markovian noise attains a better bound than the standard quantum limit (SQL) for both classical and SLD quantum bounds. This observation agrees with previous results reported using semidefinite programming[62], indicating the potential of variational optimization for designing optimal non-Markovian metrology experiments. Finally, we note that in the Ornstein-Uhlenbeck model, the SLD quantum bound is unachievable, as indicated by $C_F > C_S$. It remains a question for future research on whether one can attain the SLD quantum bound C_S with probe designs, and the existence of tight bounds in the non-Markovian scenario.

Discussion

Concentratable entanglement

We discuss how the three ansatzes create entangled states and the role of entangled resources in achieving the SLD quantum bound in VQM. We analyze entanglement using the concentratable entanglement (CE) defined by[63]

$$\xi(\psi) = 1 - \frac{1}{2^{|s|}} \sum_{\alpha \in \mathcal{P}(s)} \mathrm{Tr}[\rho_\alpha^2],$$

(7)

where $\mathcal{P}(s)$ is the power set of s, $\forall s \in \{1, 2, \ldots, N\}$, and ρ_α is the reduced state of $|\psi\rangle$ in the subsystem α with $\rho_\emptyset := I$. Practically, $\xi(\psi)$ can be computed using the SWAP test circuit as stated in Ref.[63], where $\xi(\psi) = 1 - p(\mathbf{0})$, with $p(\mathbf{0})$ is the probability of obtaining $|00\cdots0\rangle$. The ability of the SWAP test to compute CE is due to the equivalence between conditional probability distribution and the definition of CE.
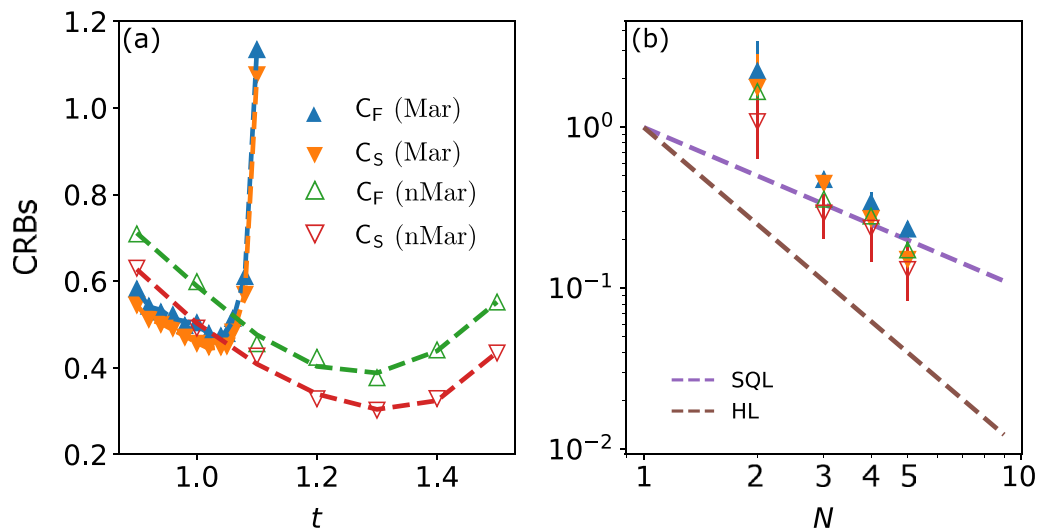

Figure 5. Variational quantum metrology under time-dephasing noise. (**a**) We present the CRBs as functions of the sensing time, demonstrating an optimal sensing time for achieving each minimum CRB. The non-Markovian dephasing (nMar) produces lower metrological bounds in comparison to the Markovian one (Mar). (**b**) Plot of the minimal bounds for cases in (**a**), comparing them with the standard quantum limit (SQL) and the Heisenberg limit (HL). For non-Markovian metrology, the bounds surpass the SQL, as predicted.

We first train the three ansatzes to evaluate their ability of entangled-state generation. Particularly, the training process aims to generate quantum states with $\xi(\psi) = \{\xi_{sep}, \xi_{GHZ}, \xi_{AME}\}$, where $\xi_{sep} = 0$ for a separable state, $\xi_{GHZ} = \frac{1}{2} - \frac{1}{2^N}$ for a GHZ state, and $\xi_{AME} = 1 - \frac{1}{2^N} \sum_{j=0}^{N} \binom{N}{j} \frac{1}{2^{\min(j, N-j)}}$ for an absolutely maximally entangled (AME) state[64,65]. The top panels in Fig. 6 display the results for star, ring, and squeezing ansatz, from left to right, at $N = 4$ and (2-2) layers of each ansatz as an example. All the ansatzes examined can reach the separable and GHZ state, but hard to achieve the AME state. This observation is consistent with the CEs for conventional graph states[65].

We next discuss the role of entanglement in achieving the ultimate SLD quantum bound. In the bottom panels of Fig. 6, we graph the corresponding CEs at the optimal CRBs shown in Fig. 3, which apparently do not require the maximum entanglement (e.g., GHZ) to achieve the ultimate SLD quantum bound. This phenomenon can be explained by the fact that maximum entanglement is not required for high-precision quantum metrology, as previously noted in Refs.[66–68]. Therefore, emphasizing the robustness of easily preparable entangled probe states and non-local POVM schemes would be advantageous for quantum metrological applications exposed to Markovian and non-Markovian noises.

Cost functions

We address the selection of the cost function used in the variational algorithm. The preference outlined in Eq. (2) is not the sole option. An alternative approach could involve adopting the classical bound C_F as the cost function to maximize the information extraction. However, this way does not guarantee the classical bound can reach the quantum bound, a requirement in estimation theory. In Fig. 7a, we present a plot depicting the cost function $\mathcal{C}(\boldsymbol{\theta}, \boldsymbol{\mu}) = C_F$ as a function of the number of iterations, considering various noise probabilities λ. It demonstrates that the cost function reaches its minimum value at a certain iteration. Correspondingly, in Fig. 7b, we provide the optimal values for both classical and quantum bounds, denoted as C'_F and C'_S, alongside this optimization. It's important to emphasize that this approach does not guarantee that C'_F equals C'_S. For comparison, we include a grayscale representation of these quantities, originally presented in Fig. 3a. Here, optimizing the cost function Eq. (2) still ensures small values and convergence for both C_F and C_S. However, C'_F and C'_S consistently remain
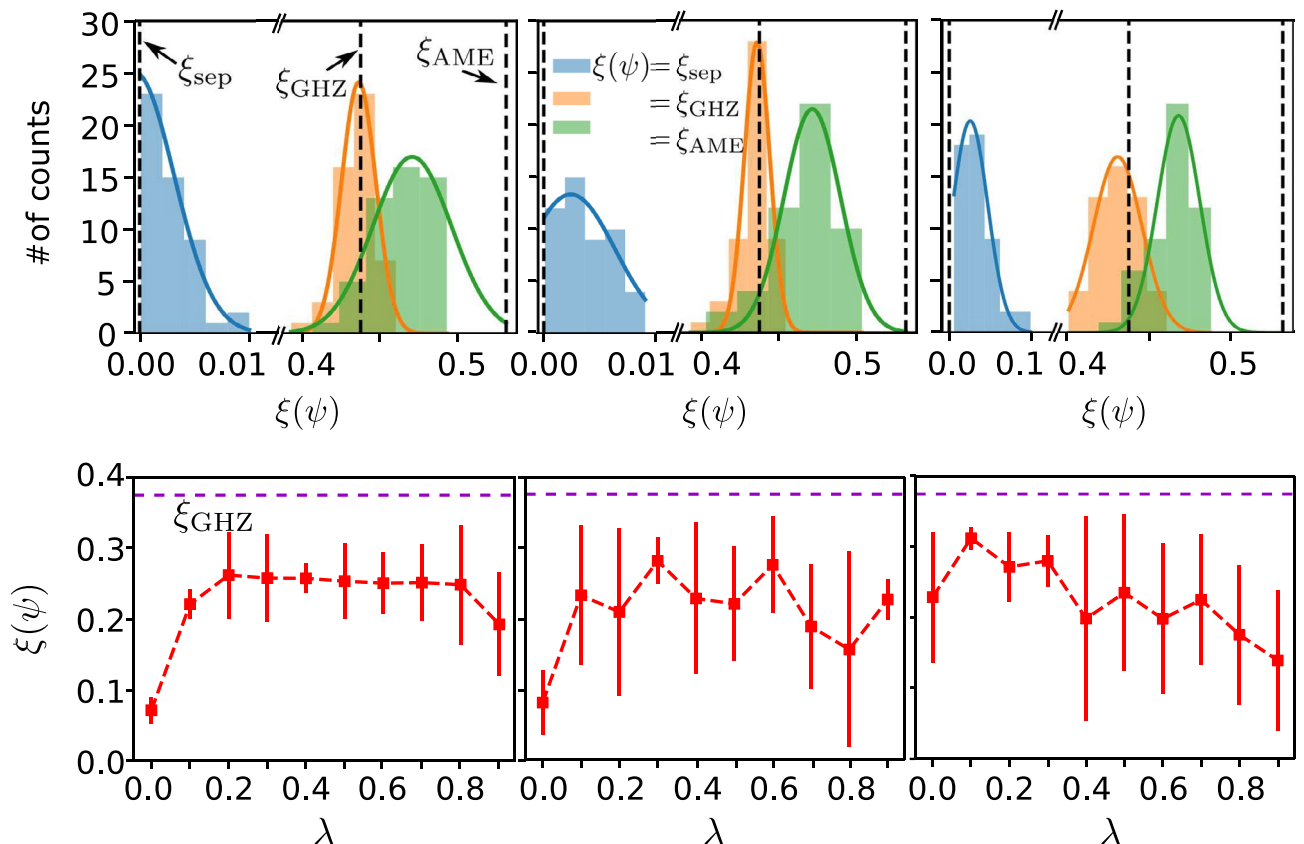

Figure 6. Entanglement generation. (Top): from left to right: the distribution of training CEs corresponds to the star, ring, and squeezing ansatzes, respectively. All the ansatzes can produce separable and GHZ states, but generating an AME state is challenging. The results are shown at $N = 4$ and (2–2) layers for each ansatz. (Bottom): the CEs are ploted at the optimal CRBs in Fig. 3, using the same circuit setup that in the figure. Again, λ is the dephasing probability.
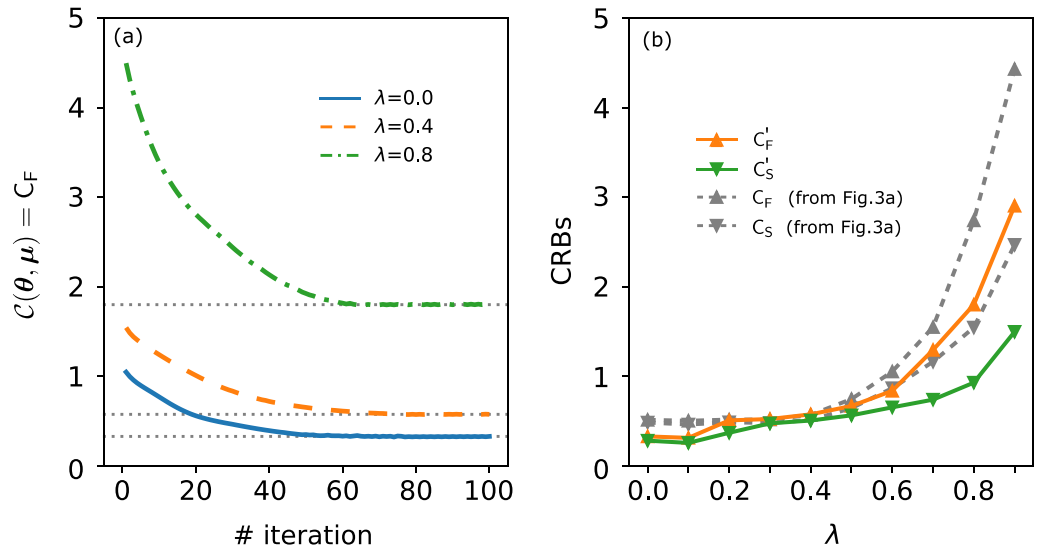
Figure 7. Optimizing classical bound C_F through Variational Quantum Metrology. (**a**) Plot of the cost function $\mathcal{C}(\boldsymbol{\theta}, \boldsymbol{\mu}) = C_F$ versus the number of iterations across various noise probabilities λ. (**b**) Plot of the corresponding optimal values of C'_F and C'_S, and their counterparts extracted from Fig. 3a (in grayscale). These numerical results pertain to the star-graph configuration.

below C_F and C_S. This behavior occurs because the evaluation of C_F and C_S is based on the state that maximizes the figure of merit in Eq. (2), rather than solely minimizing C_F or C_S.

Furthermore, alternative physical quantities, such as the tradeoff $\mathcal{T}$ and the norm-2, can also be utilized as potential cost functions. For instance, a tradeoff cost function is analogous to the one presented in Eq. (2), taking the form:

$$\mathcal{C}(\boldsymbol{\theta}, \boldsymbol{\mu}) = 1 - \frac{1}{d}\text{Tr}[FQ^{-1}], \tag{8}$$

where d is the number of estimated parameters. Notably, in scenarios where Q is a diagonal matrix and $\mathcal{C}(\boldsymbol{\theta}, \boldsymbol{\mu}) = 0$, it results in a zero tradeoff, i.e., $\frac{F_{11}}{Q_{11}} = \cdots = \frac{F_{dd}}{Q_{dd}} = 1$. Additionally, norm-2 can also function as a viable cost function[27].

$$\mathcal{C}(\boldsymbol{\theta}, \boldsymbol{\mu}) = ||F - Q||_2, \tag{9}$$

where $||A||_2 = \sqrt{\lambda_{\max}(A^*A)}$ represents the norm-2, with $\lambda_{\max}$ is the maximum eigenvalue. However, it is worth noting that these alternate cost functions might not be convex nor trainable[60]. As a result, the selection of the cost function in Eq. (2) is indeed appropriate.

Methods

Quantum circuit training

In numerical simulations, we employ the ADAM optimizer to train the VQM variables[69], where the variables at step $k + 1$ are given by

$$\boldsymbol{\theta}^{k+1} = \boldsymbol{\theta}^k - \alpha \frac{\hat{m}_k}{\sqrt{\hat{v}_k} + \epsilon}, \tag{10}$$

where $m_k = \beta_1 m_{k-1} + (1 - \beta_1)\nabla_{\boldsymbol{\theta}}\mathcal{C}(\boldsymbol{\theta}), v_k = \beta_2 v_{k-1} + (1 - \beta_2)\nabla^2_{\boldsymbol{\theta}}\mathcal{C}(\boldsymbol{\theta}), \hat{m}_k = m_k/(1 - \beta_1^k), \hat{v}_k = v_k/(1 - \beta_2^k)$, with the hyper-parameters are chosen as $\alpha = 0.2, \beta_1 = 0.8, \beta_2 = 0.999$ and $\epsilon = 10^{-8}$. The gradient $\partial_{\theta_i}\mathcal{C}(\boldsymbol{\theta})$ is given through the parameter-shift rule[70,71]. The simulations are performed in Qiskit Aer simulator[72]. The number of iterations is chosen using the EarlyStopping callback[57].

To determine the appropriate number of layers for the preparation state and POVM ansatzes, we analyze the cost function (2) with different number of layers. We use $(\star, \dagger\text{-}\ddagger)$ to denote the minimum cost function, the number of layers for variational state preparation, and the number of layers for variational POVM. The results are shown in Fig. 8 with $(\star, \dagger\text{-}\ddagger) = (0.057, 2\text{-}2), (0.04, 3\text{-}2)$, and $(0.054, 2\text{-}2)$ for the star, ring, and squeezing ansatz, respectively. Obviously, the metrological performances of these ansatzes demonstrate that deep ansatzes are unnecessary, as also noted in[46] where a shallow ansatz was able to saturate quantum bound. For the numerical simulations presented in this paper, we keep the number of layers fixed at these values.
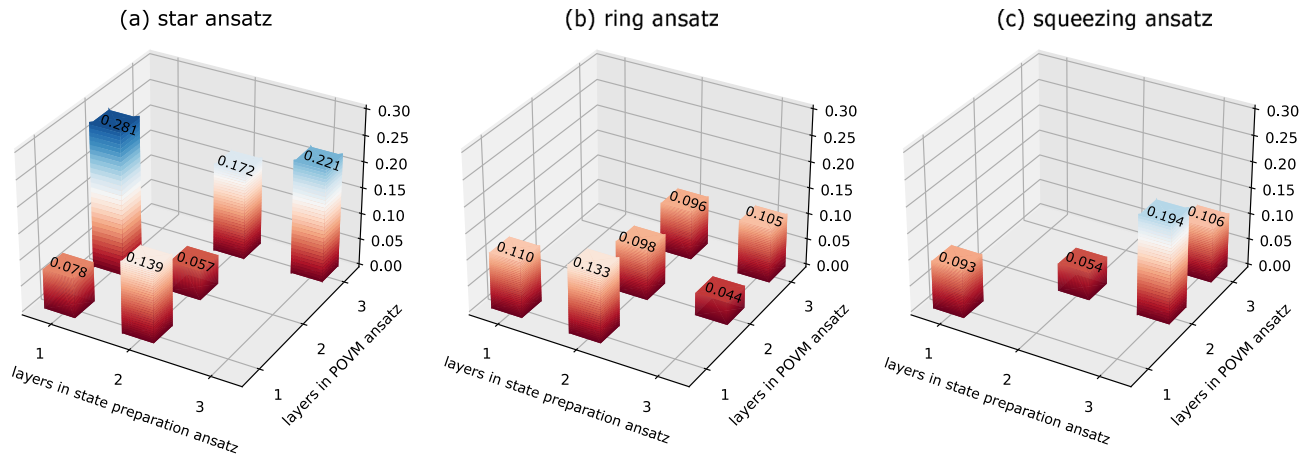
Figure 8. Cost function versus the optimal number of layers for different ansatzes. The plot of the cost function for (**a**) star ansatz, (**b**) ring ansatz, and (**c**) squeezing ansatz at $N = 3$ without noise. The minimum cost function vs the number of layers are (0.057, 2-2), (0.044, 3-2), and (0.054, 2-2), respectively.

Computing Fisher information

Classical and quantum Fisher information matrices can be computed in quantum circuits using the finite difference approximation. For the CFIM, we first derive an output probability as $\partial_{\phi_i} p = \frac{p(\phi_i+s)-p(\phi_i-s)}{2s}$, for a small shift s. We then compute the CFIM from $F_{ij} = \sum_m \frac{1}{p(m|\boldsymbol{\phi})}[\partial_{\phi_i} p(m|\boldsymbol{\phi})][\partial_{\phi_j} p(m|\boldsymbol{\phi})]$. For the QFIM, we explicitly derive $Q_{ij} = 2\text{vec}[\partial_{\phi_i}\rho(\boldsymbol{\phi})]^{\dagger}\left[\rho(\boldsymbol{\phi})^* \otimes I + I \otimes \rho(\boldsymbol{\phi})\right]^{+}\text{vec}[\partial_{\phi_j}\rho(\boldsymbol{\phi})]$, where $\text{vec}[\cdot]$ is the vectorization of a matrix, and the superscript '+' denotes the pseudo-inversion[73]. Again, we apply the finite difference to compute $\partial_{\phi_i}\rho = \frac{\rho(\phi_i+s)-\rho(\phi_i-s)}{2s}$, and substitute into the above equations to compute the QFIM.

Data availability

Data are available from the corresponding authors upon reasonable request.

Code availability

All codes used to produce the findings of this study are incorporated into `tqix`[74,75] and available at: https://github.com/echkon/tqix-developers. See also the Supplementary Material for tutorial codes.

References

1. Braunstein, S. L. & Caves, C. M. Statistical distance and the geometry of quantum states. *Phys. Rev. Lett.* **72**, 3439–3443. https://doi.org/10.1103/PhysRevLett.72.3439 (1994).
2. Giovannetti, V., Lloyd, S. & Maccone, L. Advances in quantum metrology. *Nat. Photon.* **5**, 222–229. https://doi.org/10.1038/nphoton.2011.35 (2011).
3. Tóth, G. & Apellaniz, I. Quantum metrology from a quantum information science perspective. *J. Phys. A Math. Theor.* **47**, 424006. https://doi.org/10.1088/1751-8113/47/42/424006 (2014).
4. Barndorff-Nielsen, O. E. & Gill, R. D. Fisher information in quantum statistics. *J. Phys. A Math. Gen.* **33**, 4481. https://doi.org/10.1088/0305-4470/33/24/306 (2000).
5. Fujiwara, A. Strong consistency and asymptotic efficiency for adaptive quantum estimation problems. *J. Phys. A Math. Gen.* **39**, 12489. https://doi.org/10.1088/0305-4470/39/40/014 (2006).
6. Zhang, Y.-H. & Yang, W. Improving spin-based noise sensing by adaptive measurements. *New J. Phys.* **20**, 093011. https://doi.org/10.1088/1367-2630/aadd5e (2018).
7. Demkowicz-Dobrzański, R., Czajkowski, J. & Sekatski, P. Adaptive quantum metrology under general Markovian noise. *Phys. Rev. X* **7**, 041009. https://doi.org/10.1103/PhysRevX.7.041009 (2017).
8. Kessler, E. M., Lovchinsky, I., Sushkov, A. O. & Lukin, M. D. Quantum error correction for metrology. *Phys. Rev. Lett.* **112**, 150802. https://doi.org/10.1103/PhysRevLett.112.150802 (2014).
9. Zhou, S., Zhang, M., Preskill, J. & Jiang, L. Achieving the Heisenberg limit in quantum metrology using quantum error correction. *Nat. Commun.* **9**, 78. https://doi.org/10.1038/s41467-017-02510-3 (2018).
10. Yang, J., Pang, S., Chen, Z., Jordan, A. N. & del Campo, A. Variational principle for optimal quantum controls in quantum metrology. *Phys. Rev. Lett.* **128**, 160505. https://doi.org/10.1103/PhysRevLett.128.160505 (2022).
11. Pang, S. & Jordan, A. N. Optimal adaptive control for quantum metrology with time-dependent Hamiltonians. *Nat. Commun.* **8**, 14695. https://doi.org/10.1038/ncomms14695 (2017).
12. Yang, X., Chen, X., Li, J., Peng, X. & Laflamme, R. Hybrid quantum-classical approach to enhanced quantum metrology. *Sci. Rep.* **11**, 672. https://doi.org/10.1038/s41598-020-80070-1 (2021).
13. Koczor, B., Endo, S., Jones, T., Matsuzaki, Y. & Benjamin, S. C. Variational-state quantum metrology. *New J. Phys.* **22**, 083038. https://doi.org/10.1088/1367-2630/ab965e (2020).
14. Ma, Z. *et al.* Adaptive circuit learning for quantum metrology. In 2021 IEEE International Conference on Quantum Computing and Engineering (QCE), 419–430. https://doi.org/10.1109/QCE52317.2021.00063 (2021)
15. Kaubruegger, R. *et al.* Variational spin-squeezing algorithms on programmable quantum sensors. *Phys. Rev. Lett.* **123**, 260505. https://doi.org/10.1103/PhysRevLett.123.260505 (2019).

16. Kaubruegger, R., Vasilyev, D. V., Schulte, M., Hammerer, K. & Zoller, P. Quantum variational optimization of Ramsey interferometry and atomic clocks. *Phys. Rev. X* **11**, 041045. https://doi.org/10.1103/PhysRevX.11.041045 (2021).

17. Zheng, T.-X. *et al.* Preparation of metrological states in dipolar-interacting spin systems. npj Quantum Inf. **8**, 150. https://doi.org/10.1038/s41534-022-00667-4 (2022).

18. Li, Z., Zou, L. & Hsieh, T. H. Hamiltonian tomography via quantum quench. *Phys. Rev. Lett.* **124**, 160502. https://doi.org/10.1103/PhysRevLett.124.160502 (2020).

19. Baumgratz, T. & Datta, A. Quantum enhanced estimation of a multidimensional field. *Phys. Rev. Lett.* **116**, 030801. https://doi.org/10.1103/PhysRevLett.116.030801 (2016).

20. Ho, L. B., Hakoshima, H., Matsuzaki, Y., Matsuzaki, M. & Kondo, Y. Multiparameter quantum estimation under dephasing noise. *Phys. Rev. A* **102**, 022602. https://doi.org/10.1103/PhysRevA.102.022602 (2020).

21. Hou, Z. *et al.* Minimal tradeoff and ultimate precision limit of multiparameter quantum magnetometry under the parallel scheme. *Phys. Rev. Lett.* **125**, 020501. https://doi.org/10.1103/PhysRevLett.125.020501 (2020).

22. Schnabel, R., Mavalvala, N., McClelland, D. E. & Lam, P. K. Quantum metrology for gravitational wave astronomy. *Nat. Commun.* **1**, 121. https://doi.org/10.1038/ncomms1122 (2010).

23. Derevianko, A. & Katori, H. Colloquium: physics of optical lattice clocks. *Rev. Mod. Phys.* **83**, 331–347. https://doi.org/10.1103/RevModPhys.83.331 (2011).

24. Ludlow, A. D., Boyd, M. M., Ye, J., Peik, E. & Schmidt, P. O. Optical atomic clocks. *Rev. Mod. Phys.* **87**, 637–701. https://doi.org/10.1103/RevModPhys.87.637 (2015).

25. Albarelli, F. & Demkowicz-Dobrzański, R. Probe incompatibility in multiparameter noisy quantum metrology. *Phys. Rev. X* **12**, 011039. https://doi.org/10.1103/PhysRevX.12.011039 (2022).

26. Kull, I., Guérin, P. A. & Verstraete, F. Uncertainty and trade-offs in quantum multiparameter estimation. *J. Phys. A Math. Theor.* **53**, 244001. https://doi.org/10.1088/1751-8121/ab7f67 (2020).

27. Pezzè, L. *et al.* Optimal measurements for simultaneous quantum estimation of multiple phases. *Phys. Rev. Lett.* **119**, 130504. https://doi.org/10.1103/PhysRevLett.119.130504 (2017).

28. Yang, J., Pang, S., Zhou, Y. & Jordan, A. N. Optimal measurements for quantum multiparameter estimation with general states. *Phys. Rev. A* **100**, 032104. https://doi.org/10.1103/PhysRevA.100.032104 (2019).

29. Yuan, H. Sequential feedback scheme outperforms the parallel scheme for Hamiltonian parameter estimation. *Phys. Rev. Lett.* **117**, 160801. https://doi.org/10.1103/PhysRevLett.117.160801 (2016).

30. Ho, L. B. & Kondo, Y. Multiparameter quantum metrology with postselection measurements. J. Math. Phys. **62**, 012102. https://doi.org/10.1063/5.0024555 (2021).

31. Meyer, J. J., Borregaard, J. & Eisert, J. A variational toolbox for quantum multi-parameter estimation. npj Quantum Inf. **7**, 89. https://doi.org/10.1038/s41534-021-00425-y (2021).

32. Zhu, H. Information complementarity: A new paradigm for decoding quantum incompatibility. *Sci. Rep.* **5**, 14317. https://doi.org/10.1038/srep14317 (2015).

33. Ragy, S., Jarzyna, M. & Demkowicz-Dobrzański, R. Compatibility in multiparameter quantum metrology. *Phys. Rev. A* **94**, 052108. https://doi.org/10.1103/PhysRevA.94.052108 (2016).

34. Uhlenbeck, G. E. & Ornstein, L. S. On the theory of the Brownian motion. *Phys. Rev.* **36**, 823–841. https://doi.org/10.1103/PhysRev.36.823 (1930).

35. Helstrom, C. W. *Quantum Detection and Estimation Theory* (Academic Press, New York, 1976).

36. Holevo, A. Probabilistic and Statistical Aspects of Quantum Theory (Springer, New York, 2011), 1st edn.

37. Conlon, L. O., Suzuki, J., Lam, P. K. & Assad, S. M. The gap persistence theorem for quantum multiparameter estimation (2022). arXiv:2208.07386.

38. Hayashi, M. & Ouyang, Y. Tight cramér-rao type bounds for multiparameter quantum metrology through conic programming (2023). arXiv:2209.05218.

39. Paris, M. G. A. Quantum state estimation. *Int. J. Quantum Inf.* **7**, 125–137 (2009).

40. Conlon, L. O., Suzuki, J., Lam, P. K. & Assad, S. M. Efficient computation of the Nagaoka–Hayashi bound for multiparameter estimation with separable measurements. npj Quantum Inf. **7**, 110. https://doi.org/10.1038/s41534-021-00414-1 (2021).

41. Hayashi, M. (ed.) Asymptotic Theory of Quantum Statistical Inference: Selected Papers (World Scientific Singapore, 2005).

42. Kay, S. Estimation theory, Vol 1 (Prentice Hall, Englewood Cliffs, NJ, 1993), 1st edn.

43. Yang, Y., Chiribella, G. & Hayashi, M. Attaining the ultimate precision limit in quantum state estimation. *Commun. Math. Phys.* **368**, 223–293. https://doi.org/10.1007/s00220-019-03433-4 (2019).

44. Yamagata, K., Fujiwara, A. & Gill, R. D. Quantum local asymptotic normality based on a new quantum likelihood ratio. *Ann. Stat.* **41**, 2197–2217. https://doi.org/10.1214/13-AOS1147 (2013).

45. Sidhu, J. S., Ouyang, Y., Campbell, E. T. & Kok, P. Tight bounds on the simultaneous estimation of incompatible parameters. *Phys. Rev. X* **11**, 011028. https://doi.org/10.1103/PhysRevX.11.011028 (2021).

46. Friel, J., Palittapongarnpim, P., Albarelli, F. & Datta, A. Attainability of the holevo-cramér-rao bound for two-qubit 3d magnetometry. https://doi.org/10.48550/ARXIV.2008.01502 (2020).

47. Albarelli, F., Friel, J. F. & Datta, A. Evaluating the Holevo Cramér–Rao bound for multiparameter quantum metrology. *Phys. Rev. Lett.* **123**, 200503. https://doi.org/10.1103/PhysRevLett.123.200503 (2019).

48. Demkowicz-Dobrzański, R., Górecki, W. & Guţă, M. Multi-parameter estimation beyond quantum fisher information. *J. Phys. A Math. Theor.* **53**, 363001. https://doi.org/10.1088/1751-8121/ab8ef3 (2020).

49. Matsumoto, K. A new approach to the Cramér–Rao-type bound of the pure-state model. *J. Phys. A Math. Gen.* **35**, 3111. https://doi.org/10.1088/0305-4470/35/13/307 (2002).

50. Humphreys, P. C., Barbieri, M., Datta, A. & Walmsley, I. A. Quantum enhanced multiple phase estimation. *Phys. Rev. Lett.* **111**, 070403. https://doi.org/10.1103/PhysRevLett.111.070403 (2013).

51. Shettell, N. & Markham, D. Graph states as a resource for quantum metrology. *Phys. Rev. Lett.* **124**, 110502. https://doi.org/10.1103/PhysRevLett.124.110502 (2020).

52. Wang, Y. & Fang, K. Continuous-variable graph states for quantum metrology. *Phys. Rev. A* **102**, 052601. https://doi.org/10.1103/PhysRevA.102.052601 (2020).

53. Maccone, L. & Riccardi, A. Squeezing metrology: A unified framework. *Quantum* **4**, 292. https://doi.org/10.22331/q-2020-07-09-292 (2020).

54. Gessner, M., Smerzi, A. & Pezzè, L. Multiparameter squeezing for optimal quantum enhancements in sensor networks. *Nat. Commun.* **11**, 3817. https://doi.org/10.1038/s41467-020-17471-3 (2020).

55. Carrara, G., Genoni, M. G., Cialdi, S., Paris, M. G. A. & Olivares, S. Squeezing as a resource to counteract phase diffusion in optical phase estimation. *Phys. Rev. A* **102**, 062610. https://doi.org/10.1103/PhysRevA.102.062610 (2020).

56. Mølmer, K. & Sørensen, A. Multiparticle entanglement of hot trapped ions. *Phys. Rev. Lett.* **82**, 1835–1838. https://doi.org/10.1103/PhysRevLett.82.1835 (1999).

57. Keras. Earlystopping callback - keras documentation. https://keras.io/api/callbacks/early_stopping/ (2021). [Online; accessed 28-March-2023].

58. Vidrighin, M. D. *et al.* Joint estimation of phase and phase diffusion for quantum metrology. *Nat. Commun.* **5**, 3532. https://doi.org/10.1038/ncomms4532 (2014).

59. Wang, S. *et al.* Noise-induced barren plateaus in variational quantum algorithms. *Nat. Commun.* **12**, 6961. https://doi.org/10.1038/s41467-021-27045-6 (2021).
60. Cerezo, M. *et al.* Variational quantum algorithms. *Nat. Rev. Phys.* **3**, 625–644. https://doi.org/10.1038/s42254-021-00348-9 (2021).
61. Yu, T. & Eberly, J. Entanglement evolution in a non-Markovian environment. *Opt. Commun.* **283**, 676–680. https://doi.org/10.1016/j.optcom.2009.10.042 (2010).
62. Altherr, A. & Yang, Y. Quantum metrology for non-Markovian processes. *Phys. Rev. Lett.* **127**, 060501. https://doi.org/10.1103/PhysRevLett.127.060501 (2021).
63. Beckey, J. L., Gigena, N., Coles, P. J. & Cerezo, M. Computable and operationally meaningful multipartite entanglement measures. *Phys. Rev. Lett.* **127**, 140501. https://doi.org/10.1103/PhysRevLett.127.140501 (2021).
64. Enríquez, M., Wintrowicz, I. & Życzkowski, K. Maximally entangled multipartite states: A brief survey. *J. Phys. Conf. Ser.* **698**, 012003. https://doi.org/10.1088/1742-6596/698/1/012003 (2016).
65. Cullen, A. R. & Kok, P. Calculating concentratable entanglement in graph states. *Phys. Rev. A* **106**, 042411. https://doi.org/10.1103/PhysRevA.106.042411 (2022).
66. Oszmaniec, M. *et al.* Random bosonic states for robust quantum metrology. *Phys. Rev. X* **6**, 041044. https://doi.org/10.1103/PhysRevX.6.041044 (2016).
67. Braun, D. *et al.* Quantum-enhanced measurements without entanglement. *Rev. Mod. Phys.* **90**, 035006. https://doi.org/10.1103/RevModPhys.90.035006 (2018).
68. Tilma, T., Hamaji, S., Munro, W. J. & Nemoto, K. Entanglement is not a critical resource for quantum metrology. *Phys. Rev. A* **81**, 022108. https://doi.org/10.1103/PhysRevA.81.022108 (2010).
69. Kingma, D. P. & Ba, J. Adam: A method for stochastic optimization. In Proceedings of the 3rd International Conference on Learning Representations (ICLR) (2015).
70. Mitarai, K., Negoro, M., Kitagawa, M. & Fujii, K. Quantum circuit learning. *Phys. Rev. A* **98**, 032309. https://doi.org/10.1103/PhysRevA.98.032309 (2018).
71. Schuld, M., Bergholm, V., Gogolin, C., Izaac, J. & Killoran, N. Evaluating analytic gradients on quantum hardware. *Phys. Rev. A* **99**, 032331. https://doi.org/10.1103/PhysRevA.99.032331 (2019).
72. Qiskit. Aer provider tutorial (2021).
73. Šafránek, D. Simple expression for the quantum fisher information matrix. *Phys. Rev. A* **97**, 042322. https://doi.org/10.1103/PhysRevA.97.042322 (2018).
74. Viet, N. T., Chuong, N. T., Huyen, V. T. N. & Ho, L. B. tqix.pis: A toolbox for quantum dynamics simulation of spin ensembles in dicke basis. *Comput. Phys. Commun.* **286**, 108686. https://doi.org/10.1016/j.cpc.2023.108686 (2023).
75. Ho, L. B., Tuan, K. Q. & Nguyen, H. Q. tqix: A toolbox for quantum in x: X: Quantum measurement, quantum tomography, quantum metrology, and others. *Comput. Phys. Commun.* **263**, 107902. https://doi.org/10.1016/j.cpc.2021.107902 (2021).

Acknowledgements

Author contributions

T.K.L. wrote the initial code and implemented the numerical simulation. L.B.H. derived the theoretical framework, implemented the numerical simulation, and analyzed the results. L.B.H. and H.Q.N supervised the work. All authors discussed and wrote the manuscript.

Competing interests

The authors declare no competing interests.

Additional information

Supplementary Information The online version contains supplementary material available at https://doi.org/10.1038/s41598-023-44786-0.

Correspondence and requests for materials should be addressed to L.B.H.

Reprints and permissions information is available at www.nature.com/reprints.

Publisher's note Springer Nature remains neutral with regard to jurisdictional claims in published maps and institutional affiliations.